JOURNAL OF CHEMICAL INFORMATION AND MODELING

Article

pubs.acs.org/jcim

# Feasibility of Using Molecular Docking-Based Virtual Screening for Searching Dual Target Kinase Inhibitors

Shunye Zhou,[†] Youyong Li,[†] and Tingjun Hou*[,†,‡]

[†]Institute of Functional Nano & Soft Materials (FUNSOM) and Jiangsu Key Laboratory for Carbon-Based Functional Materials & Devices, Soochow University, Suzhou, Jiangsu 215123, China

[‡]College of Pharmaceutical Sciences, Zhejiang University, Hangzhou, Zhejiang 310058, China

Supporting Information

**ABSTRACT:** Multitarget agents have been extensively explored for solving limited efficacies, poor safety, and resistant profiles of an individual target. Theoretical approaches for searching and designing multitarget agents are critically useful. Here, the performance of molecular docking to search dual-target inhibitors for four kinase pairs (CDK2-GSK3B, EGFR-Src, Lck-Src, and Lck-VEGFR2) was assessed. First, the representative structures for each kinase target were chosen by structural clustering of available crystal structures. Next, the performance of molecular docking to distinguish inhibitors from noninhibitors for each individual kinase target was evaluated. The results show that molecular docking-based virtual screening illustrates good capability to find known inhibitors for individual targets, but the prediction accuracy is structurally dependent. Finally, the performance of molecular docking to identify the dual-target kinase inhibitors for four kinase pairs was evaluated. The analyses show that molecular docking successfully filters out most noninhibitors and achieves promising performance for identifying dual-kinase inhibitors for CDK2-GSK3B and Lck-VEGFR2. But a high false-positive rate leads to low enrichment of true dual-target inhibitors in the final list. This study suggests that molecular docking serves as a useful tool in searching inhibitors against dual or even multiple kinase targets, but integration with other virtual screening tools is necessary for achieving better predictions.

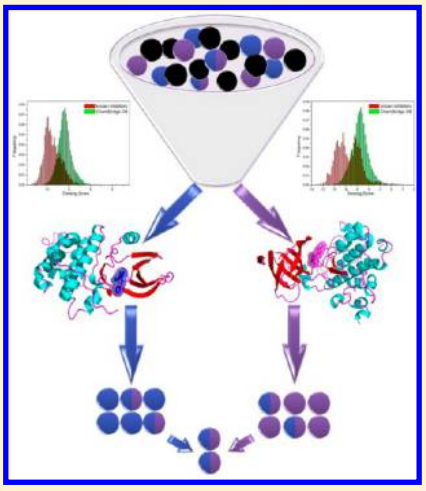

## INTRODUCTION

Over the past decades, designing highly selective drug candidates against an individual target has become the primary strategy of drug discovery.[1] However, many complex diseases such as cancers are not completely modulated by a single target. Moreover, the efficacy of a single-target drug for treating complex diseases might be compromised by the redundancies in signaling pathway.[2] Therefore, the design of drugs modulating intended multiple targets simultaneously has attracted increasing attention.[3] Currently, there are two contrasting strategies for multitarget therapeutics. Combination drug therapy is the first strategy by creating an additive or synergistic effect of multiple drugs acting on separate targets. The second strategy of multitarget therapeutics involves discovering a single agent that can act on two or more targets simultaneously. It is believed that the second strategy is more important because the pharmacokinetics and pharmacodynamics of a single agent are more predictable than those of two or more agents.[4−7]

More and more agents have been successfully designed or discovered to modulate the activity of multiple targets.[2] Particularly, the design of multikinase inhibitors with required bioactivity profiles is currently an area of great interest in the pharmaceutical industry, especially for the treatment of cancers. Several multitarget kinase drugs are already in clinical use, such as imatinib against Bcr and Abl,[8] sunitinib against PDGFR and VEGFR,[9] sorafenib against VEGFR, PDGFR, B-Raf, and C-Raf,[10] dasatinib against BCR, Abl, and Src,[11] lapatinib against EGFR and HER2,[12] etc. The high degree of sequence and structural homology among the ATP-binding pockets of kinases makes it plausible to design agents against multiple kinases.[13,14] In the meanwhile, how to minimize the cross-reactivity with untended kinase targets is a big challenge.

High-throughput screening (HTS) experiments measure bioactivity profiles of compound collections against a set of protein kinases.[15−18] Especially the kinase panel technology has emerged as a promising approach to address the cross-reactivity issue.[19,20] However, experimental identification of multitarget bioactivity profiles for large-scale compound libraries is expensive and time-consuming, and in silico modeling approaches to search multitarget agents are urgently demanded. Recently, several computational methods or protocols have been proposed to predict the kinase bioactivity profiles for large-scale compound libraries or screen selective multitarget kinase inhibitors based on quantitative structure activity relationship (QSAR) modeling or machine learning approaches.[21−28]

**Received:** January 28, 2013
**Published:** March 18, 2013

   dx.doi.org/10.1021/ci400065e | J. Chem. Inf. Model. 2013, 53, 982−996

Most of the computational approaches for predicting kinase bioactivity profiles are ligand-based, not target-based. Target-based approaches, especially molecular docking, have already become mainstream for computer-aided drug design (CADD) when target structures are available. However, the accurate prediction of selectivity and cross-reactivity on a kinomewide scale by using molecular docking is challenging because the ATP-pockets of most kinases are highly conserved in sequence and structure. Moreover, the kinase ATP-pockets usually undergo large conformational change upon association with ligands, which cannot be well captured by docking-based algorithms.

The capability of molecular docking approaches in searching active compounds against individual kinase targets from compound libraries has been extensively explored,[29,30] but their capability for searching multikinase agents from compound libraries has not been evaluated. Here, we aimed to evaluate the performance of molecular docking-based virtual screening to search inhibitors that can target two kinases. Four kinase pairs, including CDK2-GSK3B, EGFR-Src, Lck-Src, and Lck-VEGFR2, were used in our study, and the crystal structures of all the six studied kinase targets are already available. These four kinase pairs are frequently coexpressed or coactivated in various cancers[28] and have an abundant number of dual inhibitors. These four kinase pairs were also studied by Ma and co-workers.[28] In this study, considering that the same protein kinase shows different 3D crystal structures, clustering based on the structural alignments of the binding sites were employed to select the most representative structures for molecular docking. Then, molecular docking-based virtual screening was performed for each kinase target, and the capability to distinguish inhibitors from noninhibitors was evaluated. Finally, based on the predictions for individual targets, the prediction accuracy of molecular docking to identify the dual-kinase inhibitors for four kinase pairs was assessed.

## MATERIALS AND METHODS

**Compilation of Data.** The inhibitors for CDK2 (2348), GSK3B (1503), EGFR (3160), Src (959), Lck (238), and VEGFR (3368) were collected from the BindingDB database,[31] and the dual inhibitors were then determined for the CDK2-GSK3B (282), EGFR-Src (185), Lck-Src (52), and Lck-VEGFR2 (112) pairs. The dual inhibitors for each kinase pair refer to the inhibitors that target the two kinases regardless of their activities against the others.[28] The molecules randomly selected from the ChemBridge Database[32] were used as noninhibitors for molecular docking-based virtual screening.

The 3D crystal structures of each kinase for molecular docking were retrieved from the Protein Data Bank (PDB).[33] Only the crystal structures that include both receptor and ligand were retained. To eliminate redundancy, only one crystal structure was retained for each paper.

**Structural Clustering of the Crystal Structures for Each Target.** It is well-known that each protein crystal structure is just a snapshot of a flexible protein, and it cannot describe the flexibility of a protein.[34] Moreover, the binding site of a kinase may undergo conformational change upon association with a ligand. Therefore, for the same kinase target, the conformations of the binding sites in different crystal structures may be quite different. Here, a structural clustering protocol based on the structural alignments of the binding pockets was designed to determine the representative structures for molecular docking: (1) first, the ATP-binding pocket residues were defined as the protein residues within 10 Å of the ligand; (2) then, the crystal structures for each kinase target were structurally aligned based on the binding pocket residues using the STAMP algorithm[35] in VMD;[36] (3) finally, the phylogenetic tree for each kinase was generated by using the *Create Phylogenetic Tree* module in VMD based on the scores of structural similarity. According to the phylogenetic tree, the representative structures with the largest structural diversity of the ATP-binding pockets were determined.

**Protein Preparation.** The crystal structures selected by structural clustering were used as the templates in the docking calculations performed with Glide in Schrödinger 9.0.[37] Then, the *Protein Preparation Wizard* in Schrödinger 9.0 was used to remove crystallographic water molecules, add hydrogen atoms, assign partial charges using the OPLS-2005 force field,[38] assign protonation states, and minimize the structure.[39] The minimization was terminated when the root-mean-square deviation (RMSD) reached a maximum value of 0.3 Å.

**Ligand Preparation.** For each target, a noninhibitor set was artificially generated by choosing molecules from the ChemBridge data set. It is well-known that only a small portion of small molecules are kinase inhibitors. To mimic the unbalanced nature of inhibitors versus noninhibitors in the chemical space, we chose to set the ratio of inhibitors versus noninhibitors to 20 when generating the noninhibitor set. The protocol used in ligand preparation is shown in Figure S1 in the Supporting Information. First, for each kinase target, the Tanimoto similarity between each ChemBridge molecule and each inhibitor was calculated in Discovery Studio 2.5[40] based on the FCFP_6 fingerprints,[41] and the ChemBridge molecule that shows Tanimoto similarity coefficient larger than 0.45 to any kinase inhibitor was removed from ChemBridge. Then, a noninhibitor set was extracted using the *Find Diverse Molecules* protocol in Discovery Studio 2.5, and they have the largest diversity evaluated by the Tanimoto distance for the FCFP_4 fingerprints.[41]

The inhibitors and noninhibitors for each target were preprocessed by the *LigPrep* module in Schrödinger 9.0.[42] The ionized states and tautomers were generated using *Epik* at pH = 7.0.[42] The original chiralities were retained for the inhibitors with known 3D structures, and the different combinations of chiralities were generated for the noninhibitors without 3D structures (the maximum number of the stereoisomers for each molecule was set to 32); the lowest energy ring conformation was generated for each molecule.

**Molecular Docking Calculations.** All structures were docked into the active site of each kinase using the Glide[43] module in Schrödinger with the extra precision (XP) scoring mode. The docking grid box was generated by the *Receptor Grid Generation* module. The van der Waals radius scaling factor for protein was set to 0.8, and the cutoff for absolute partial charges was set to 0.25. In molecular docking, five thousand poses per ligand were generated during the initial phase of the docking calculation, out of which the best 1000 poses per ligand were chosen for energy minimization by 1000 steps of conjugate gradient minimizations. In the docking process of Glide, the protein conformation was fixed while the docked ligand was flexible. The best binding pose for each molecule was saved for the further analysis.

**Performance of Molecular Docking for Individual Targets.** The inhibitors and noninhibitors for each target were classified by the Recursive Partitioning (RP) technique in Discovery Studio 2.5[40] based on the Glide XP docking scores.


dx.doi.org/10.1021/ci400065e | J. Chem. Inf. Model. 2013, 53, 982−996

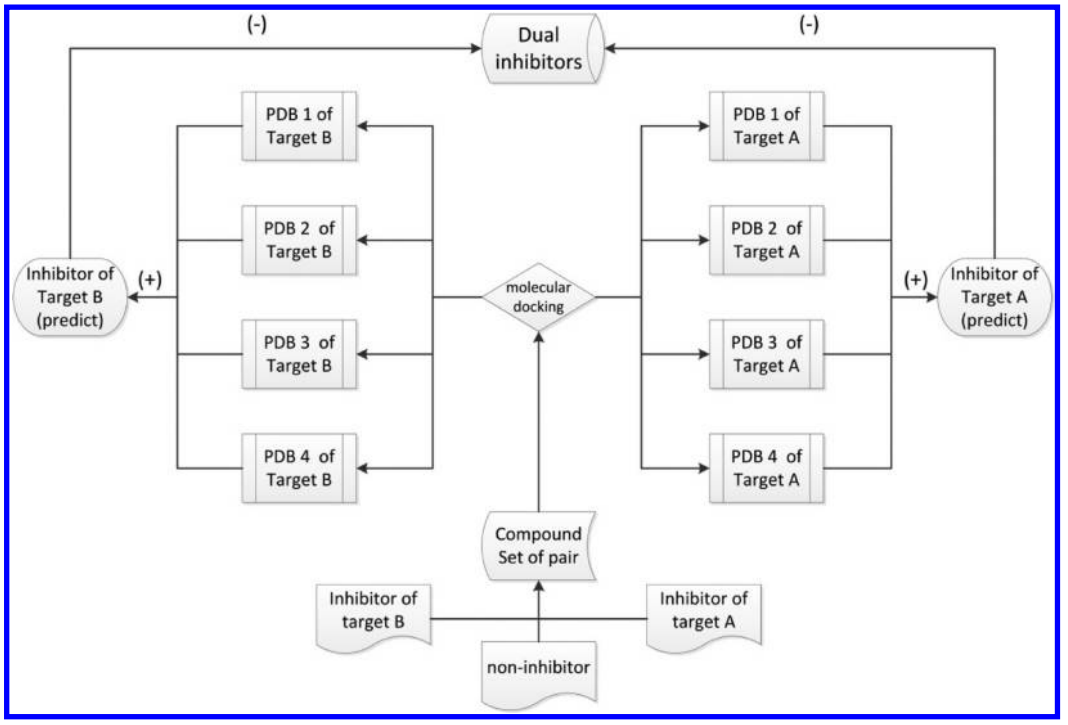


**Figure 1.** Flowchart of the docking-based protocol to find dual-target inhibitors models. (+) and (−) represent union set and intersection set, respectively.

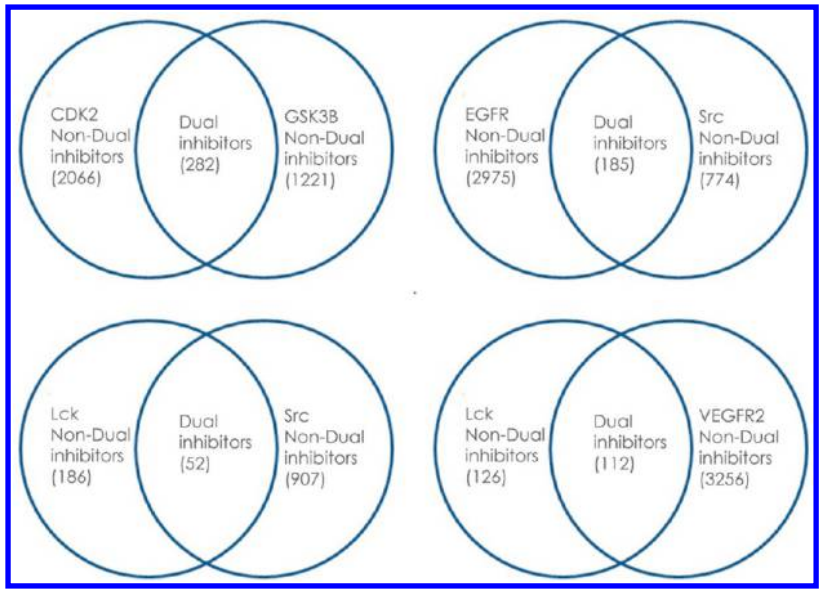


**Figure 2.** Venn graph of the collected dual-target and nondual-target inhibitors for four kinase pairs.

In classification, the inhibitor class was indicated by 1 and the noninhibitor class by 0. The classification capability was measured by the receiver operating characteristic (ROC) curve that is a graphical plot to illustrate the performance of a binary classifier as its discrimination threshold is changed. The area under ROC curve (AUC), global prediction accuracy (GA), and Matthews correlation coefficient ($C$) are three important indicators for assessing the classification capability of molecular docking. Moreover, several other important parameters for classification evaluation, including true positives (TP), false positives (FP), false negatives (FN), true negatives (TN), sensitivity (SE), and specificity (SP), were also calculated.

$$\mathrm{SE} = \frac{\mathrm{TP}}{\mathrm{TP} + \mathrm{FN}}$$

$$\mathrm{SP} = \frac{\mathrm{TN}}{\mathrm{TN} + \mathrm{FP}}$$

$$\mathrm{GA} = \frac{\mathrm{TP} + \mathrm{TN}}{\mathrm{TP} + \mathrm{FP} + \mathrm{FN} + \mathrm{TN}}$$

$$C = \frac{\mathrm{TP} \times \mathrm{TN} - \mathrm{FN} \times \mathrm{FP}}{\sqrt{(\mathrm{TP} + \mathrm{FN})(\mathrm{TP} + \mathrm{FP})(\mathrm{TN} + \mathrm{FN})(\mathrm{TN} + \mathrm{FP})}}$$

**Performance of Molecular Docking to Search Dual-Kinase Inhibitors.** After evaluating the performance of


dx.doi.org/10.1021/ci400065e | J. Chem. Inf. Model. 2013, 53, 982−996

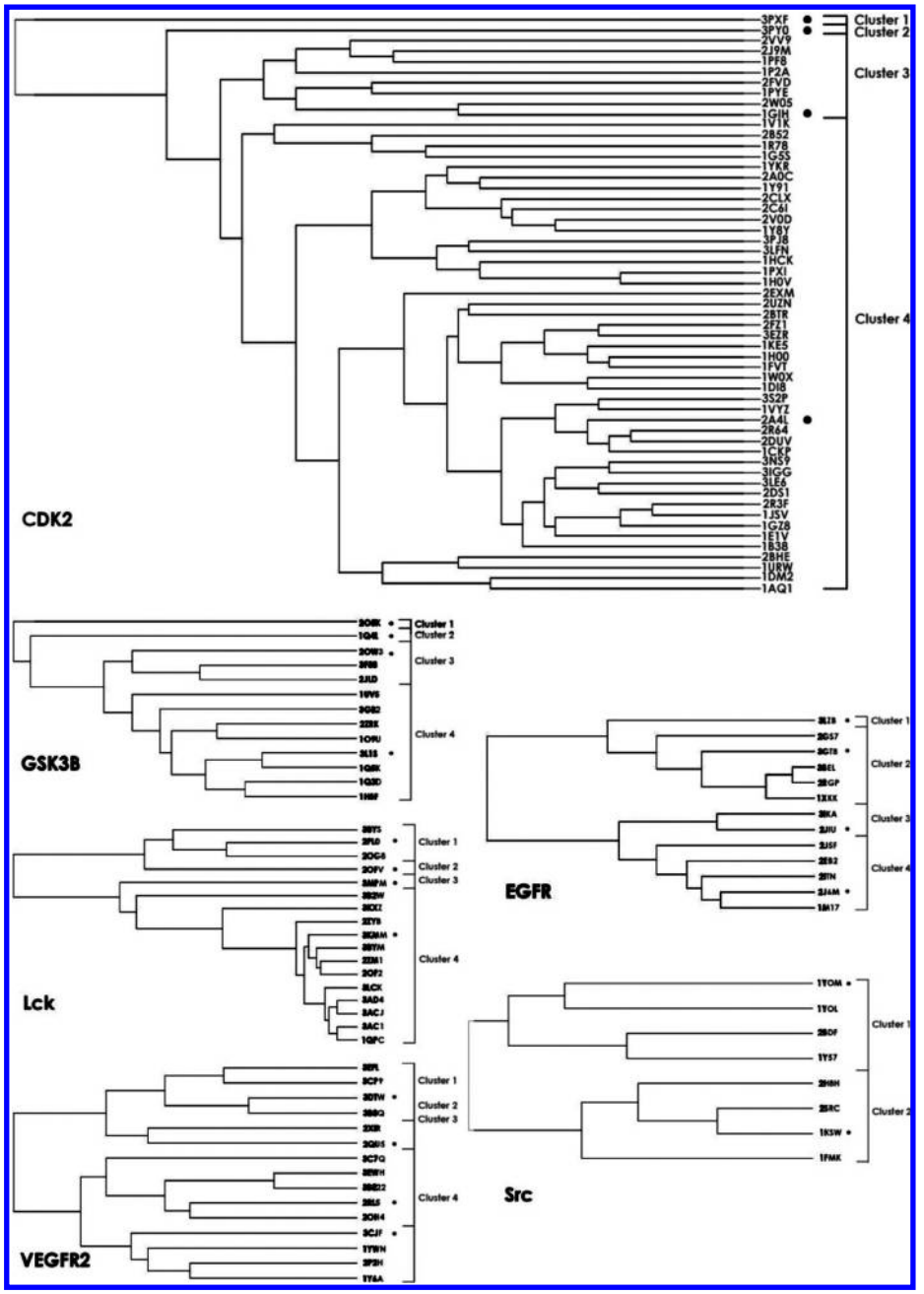


**Figure 3.** Structure-based clustering of the binding sites for the six protein kinases. The crystal structures we selected are marked with a dot.

molecular docking for individual targets, the performance of molecular docking to search dual-kinase inhibitors was evaluated for four kinase pairs. The evaluation protocol is shown in Figure 1. For each kinase pair (A and B), the inhibitors of the two kinases and 20 000 noninhibitors randomly selected from the ChemBridge data set were docked into the binding sites of targets A and B, respectively. For each kinase pair, the docked molecules can be divided into four classes: the noninhibitors for targets A and B (class 0), the inhibitors of target A but not B (class 1), the inhibitors of target B but not A (class 2), and the dual inhibitors of targets A and B (class 3). According to the thresholds given by the RP models in the previous section, we determine the category (inhibitor or noninhibitor) for each molecule based on its XP docking score. However, we found that based on the thresholds given by the RP models the predictions produce high false hit rates. Then, we used a more stringent criterion to distinguish inhibitors from noninhibitors: the top 5% of the structures ranked by the XP docking score for any protein of a target were considered as inhibitors. If a molecule is predicted as the inhibitor for the two kinases in a kinase pair, it is a potential dual-kinase inhibitor for this kinase pair. The performance of molecular docking to search dual-kinase inhibitors was evaluated by true positives (TP), false positives (FP), false negatives (FN), true negatives (TN), the yield (sensitivity), and prediction accuracy for true dual inhibitors.

$$\mathrm{Acc} = \frac{\mathrm{TP}}{\mathrm{TP} + \mathrm{FP}}$$


dx.doi.org/10.1021/ci400065e | J. Chem. Inf. Model. 2013, 53, 982−996

Table 1. Performance for the RP Models Based on the XP Docking Scores

| | TP | TN | FN | FP | SE | SP | C | GA (%) | ROC | cutoff[a] | RMSD[b] |
|---|---|---|---|---|---|---|---|---|---|---|---|
| CDK2 | | | | | | | | | | | |
| 1GIH | 1777 | 40285 | 601 | 7385 | 0.747 | 0.845 | 0.326 | 0.840 | 0.857 | −7.728 | 0.352 |
| 2A4L | 1637 | 37918 | 748 | 9907 | 0.686 | 0.793 | 0.242 | 0.788 | 0.800 | −7.308 | 1.240 |
| 3PXF | 1668 | 31321 | 660 | 15029 | 0.716 | 0.676 | 0.176 | 0.678 | 0.496 | −9.940 | 0.315 |
| 3PY0 | 1675 | 36217 | 669 | 9885 | 0.715 | 0.786 | 0.252 | 0.782 | 0.815 | −6.942 | 1.529 |
| EGFR | | | | | | | | | | | |
| 2J6M | 2038 | 51225 | 1138 | 13263 | 0.642 | 0.794 | 0.220 | 0.787 | 0.773 | −6.273 | 1.891 |
| 2JIU | 1964 | 57954 | 1211 | 6538 | 0.619 | 0.899 | 0.330 | 0.885 | 0.820 | −7.058 | 0.619 |
| 3GT8 | 1934 | 50605 | 1241 | 13819 | 0.609 | 0.785 | 0.197 | 0.777 | 0.767 | −7.337 | 2.431 |
| 3LZB | 2082 | 39483 | 1092 | 24820 | 0.656 | 0.614 | 0.117 | 0.616 | 0.679 | −6.334 | 2.734 |
| GSK3B | | | | | | | | | | | |
| 1Q4L | 775 | 26142 | 704 | 3595 | 0.524 | 0.879 | 0.247 | 0.862 | 0.760 | −7.381 | 0.375 |
| 2O5K | 924 | 21754 | 577 | 8179 | 0.616 | 0.727 | 0.161 | 0.721 | 0.722 | −5.713 | 1.839 |
| 2OW3 | 811 | 26419 | 684 | 3541 | 0.542 | 0.882 | 0.261 | 0.866 | 0.743 | −7.252 | 0.644 |
| 3L1S | 826 | 26314 | 674 | 3609 | 0.551 | 0.879 | 0.263 | 0.864 | 0.780 | −7.627 | 0.845 |
| Lck | | | | | | | | | | | |
| 2OFV | 155 | 3811 | 82 | 816 | 0.654 | 0.824 | 0.257 | 0.815 | 0.779 | −7.681 | 0.361 |
| 2PL0 | 193 | 3192 | 45 | 1542 | 0.811 | 0.614 | 0.217 | 0.681 | 0.801 | −6.284 | 1.102 |
| 3KMM | 184 | 3690 | 54 | 1051 | 0.773 | 0.778 | 0.272 | 0.778 | 0.856 | −6.593 | 1.751 |
| 3MPM | 149 | 3142 | 89 | 1592 | 0.616 | 0.664 | 0.130 | 0.662 | 0.678 | −6.600 | 0.875 |
| Src | | | | | | | | | | | |
| 1KSW | 548 | 12833 | 396 | 6487 | 0.581 | 0.664 | 0.108 | 0.660 | 0.661 | −7.452 | 1.642 |
| 1YOM | 659 | 11983 | 285 | 7343 | 0.698 | 0.620 | 0.137 | 0.624 | 0.716 | −4.962 | 1.575 |
| VEGFR2 | | | | | | | | | | | |
| 2QU5 | 1550 | 54973 | 1802 | 11331 | 0.462 | 0.829 | 0.161 | 0.811 | 0.683 | −8.820 | 0.261 |
| 2RL5 | 2072 | 56370 | 1308 | 11021 | 0.613 | 0.836 | 0.247 | 0.826 | 0.786 | −8.020 | 0.360 |
| 3CJF | 2418 | 46569 | 953 | 20948 | 0.717 | 0.690 | 0.184 | 0.691 | 0.782 | −6.592 | 3.079 |
| 3DTW | 1650 | 55452 | 1716 | 11494 | 0.490 | 0.828 | 0.174 | 0.812 | 0.699 | −8.050 | 0.344 |

[a]Cutoff of the XP docking score given by RP. [b]RMSD between the conformation of the ligand in the original crystal structure and the redocked pose.

## RESULTS AND DISCUSSION

**Preparation of Proteins and Ligands.** As shown in Figure 2, the numbers of the dual inhibitors and nondual inhibitors for the kinase pairs are 282, 2066, and 1221 for CDK2-GSK3B, 185, 2975, and 774 for EGFR-Src, 52, 186, and 907 for Lck-Src, and 112, 126, and 3256 for Lck-VEGFR, respectively. In the PDB database, one kinase usually has multiple crystal structures in complex with different ligands. For example, the numbers of crystal structures are 55 for CDK2, 13 for EGFR, 13 for GSK3B, 17 for Lck, 9 for Src, and 15 for VEGFR2. Therefore, we need to compare the ATP-binding pockets of these crystal structures for each kinase and choose the most representative structures for molecular docking. The importance of employing multiple protein structures for molecular docking has been discussed extensively.[34,44,45]

According to the results of the structural clustering shown in Figure 3, we observe that the multiple crystal structures of the same kinase are roughly divided into four clusters. Src has less crystal structures than the other kinases, and only two clusters were identified. The structure with the highest resolution in each cluster is highlighted in Figure 3. Therefore, 1GIH, 2A4L, 3PXF, and 3PY0 for CDK2, 2J6M, 2JIU, 3GT8, and 3LZB for EGFR, 1Q4L, 2O5K, 2OW3, and 3L1S for GSK3B, 2OFV, 2PL0, 3KMM, and 3MPM for Lck, 1KSW and 1YOM for Src, and 2QU5, 2RL5, 3CJF, and 3DTW for VEGFR2 were chosen as the templates for molecular docking calculations.

**Performance of Molecular Docking for Individual Kinases.** First, the performance of molecular docking was evaluated by comparing the docked binding poses with the experimental structures for the inhibitors in the X-ray cocrystallized complexes as shown in Table 2. The inhibitors in the X-ray cocrystallized complexes were redocked into the binding sites and the conformations with the lowest Glide docking scores were adopted as the binding poses. As seen from Table 1, with the exception of 3CJF, 3GT8, and 3LZB, all redocked poses agree well with the X-ray cocrystallized poses (RMSD $\leq$ 2.0 Å). The distributions of the Glide XP scores for the inhibitor and noninhibitor classes are shown in Figure 4. It is obvious that for most systems the Glide XP scores can distinguish inhibitors from noninhibitors efficiently. To give more quantitative evaluation, the ROC curves were generated (Figure 5). The ROC AUC values and the other measurements for evaluating classification are summarized in Table 1. The ROC values for three systems (CDK2, EGFR, and Lck) are higher than 0.8; that is to say, the Glide docking successfully distinguishes the true inhibitors from the noninhibitors for these systems. For two systems (GSK3b and VEGFR2), the ROC AUC values are around 0.78 and 0.79, respectively, suggesting that molecular docking is still successful to distinguish inhibitors from noninhibitors. For Src, the performance of molecular docking is not quite satisfactory, and its ROC AUC is about 0.72.

The analysis of the data in Table 1 shows that for the same target the performance of molecular docking based on different crystal structures is quite different. For example, for CDK2, the ROC AUC of 1GIH is about 0.86, while that of 3PXF is only about 0.50. That is to say, when 3PXF was used as the template the predictions of molecular docking do not have any capability


dx.doi.org/10.1021/ci400065e | J. Chem. Inf. Model. 2013, 53, 982−996

Table 2. Performance of Molecular Docking for Identifying Dual-Inhibitors for the CDK2-GSK3, EGFR-Src, Lck-Src, and Lck-VEGFR2 Kinase Pairs

| | | total | non[a] | target 1[b] | target 2[c] | dual[d] | yield (%) | Acc (%) |
|---|---|---|---|---|---|---|---|---|
| CDK2-GSK3B | exp | 23569 | 20000 | 2066 | 1221 | 282 | | |
| (1GIH-3L1S) | PR | 2208 | 644 | 1032 | 416 | 116 | 41.1 | 5.25 |
| | 10% | 1243 | 196 | 698 | 258 | 91 | 32.3 | 7.32 |
| | 5% | 522 | 31 | 285 | 155 | 51 | 18.1 | 9.77 |
| | 3% | 255 | 8 | 128 | 102 | 17 | 6.03 | 6.67 |
| CDK2-GSK3B | PR | 6380 | 3734 | 1669 | 744 | 233 | 82.6 | 3.65 |
| (multiple) | 10% | 2845 | 886 | 1281 | 516 | 162 | 57.4 | 5.69 |
| | 5% | 1379 | 219 | 747 | 309 | 104 | 36.9 | 7.54 |
| | 3% | 782 | 59 | 441 | 210 | 72 | 25.5 | 9.21 |
| EGFR-Src | exp | 23934 | 20000 | 2975 | 774 | 185 | | |
| (2JIU-1YOM) | PR | 3447 | 1505 | 1624 | 244 | 74 | 40.0 | 2.15 |
| | 10% | 970 | 104 | 734 | 79 | 23 | 12.4 | 2.37 |
| | 5% | 376 | 16 | 328 | 26 | 6 | 3.24 | 1.60 |
| | 3% | 156 | 14 | 135 | 7 | 0 | 0.00 | 0.00 |
| EGFR-Src | PR | 10421 | 7316 | 2424 | 565 | 116 | 62.7 | 1.11 |
| (multiple) | 10% | 2406 | 906 | 1278 | 179 | 43 | 23.2 | 1.79 |
| | 5% | 1039 | 241 | 694 | 85 | 19 | 10.3 | 1.83 |
| | 3% | 583 | 100 | 416 | 55 | 12 | 6.49 | 2.06 |
| Lck-Src | exp | 21145 | 20000 | 186 | 907 | 52 | | |
| (2PL0-1YOM) | PR | 5556 | 4970 | 102 | 481 | 3 | 5.77 | 0.05 |
| | 10% | 464 | 332 | 14 | 117 | 1 | 1.92 | 0.22 |
| | 5% | 161 | 95 | 3 | 62 | 1 | 1.92 | 0.62 |
| | 3% | 79 | 41 | 1 | 36 | 1 | 1.92 | 1.27 |
| Lck-Src | PR | 9251 | 8385 | 155 | 706 | 5 | 9.62 | 0.05 |
| (multiple) | 10% | 2004 | 1595 | 94 | 313 | 2 | 3.85 | 0.10 |
| | 5% | 756 | 512 | 73 | 170 | 1 | 1.92 | 0.13 |
| | 3% | 378 | 208 | 61 | 108 | 1 | 1.92 | 0.27 |
| Lck-VEGFR2 | exp | 23494 | 20000 | 126 | 3256 | 112 | | |
| (2PL0-2RL5) | PR | 3311 | 1660 | 59 | 1546 | 46 | 41.1 | 1.39 |
| | 10% | 889 | 220 | 5 | 627 | 37 | 33.0 | 4.16 |
| | 5% | 468 | 62 | 3 | 369 | 34 | 30.4 | 7.26 |
| | 3% | 183 | 8 | 3 | 145 | 27 | 24.1 | 14.8 |
| Lck-VEGFR2 | PR | 6486 | 3782 | 109 | 2508 | 87 | 77.7 | 1.34 |
| (multiple) | 10% | 3584 | 1411 | 99 | 1999 | 75 | 67.0 | 2.09 |
| | 5% | 1736 | 336 | 69 | 1267 | 64 | 57.1 | 3.69 |
| | 3% | 981 | 103 | 44 | 779 | 55 | 49.1 | 5.61 |

[a]Noninhibitors for both targets A and B. [b]Inhibitor of target A but noninhibitor of target B. [c]Inhibitor of target B but noninhibitor of target A. [d]Dual-inhibitor of targets A and B.

to distinguish inhibitors from noninhibitors. Therefore, it is obvious that the relative effectiveness of molecular docking, as measured by the ROC AUC, is highly dependent on the particular crystal structure. This finding is also consistent with the previous observations reported by Sheridan et al.,[46] Santiago et al.,[47] and Bottegoni et al.[48]

In order to understand the impact of different crystal structures of the same kinase on the performance of molecular docking, the crystal structures with the best and worst performance for each kinase target were compared and analyzed.

**CDK2 Kinase.** As shown by the Connolly surface in Supporting Information Figure S3a, the inhibitor (1PU) in 1GIH and that (2AN) in 3PXF do not bind to the same area of the binding pocket. Different from the ATP-binding site in 1GIH, the inhibitor in 3PXF was found to bind in the allosteric binding pocket.[49] However, in our calculations, the allosteric inhibitor 2AN in 3PXF was used as the anchor to define the docking grid and then all molecules were docked into the allosteric site. It is well-known that almost all known inhibitors of kinases are ATP-competitive inhibitors, and therefore, it is straightforward to understand why the molecular docking calculations based on 3PXF cannot give valid predictions. Here we also docked all molecules into the ATP-binding site of 3PXF. Unfortunately, as shown in Figure S4 in the Supporting Information the docking scores still cannot distinguish inhibitors from noninhibitors effectively. The volume of the 3PXF ATP-binding pocket measured by SiteMap in Schrödinger 9.0[42] is only 236.67 Å$^3$, which is significantly smaller than those of the others (383.13 Å$^3$ for 1GIH, 431.84 Å$^3$ for 2A4L, and 362.21 Å$^3$ for 3PY0). Therefore, it appears that the 3PXF ATP-binding pocket is too small to accommodate the available inhibitors used in our study.

**EGFR Kinase.** The schematic representation of the interactions in Supporting Information Figure S3b shows that the inhibitor (ITI) in 3LZB forms four H-bonds with the residues Lys721, Met769, and Thr830, and the inhibitor (AEE) in 2JIU forms two H-bonds with the residue Met793. Moreover, $\sigma-\pi$ interaction was found between the benzene ring of AEE and Lys745. By comparing the Connolly surfaces


dx.doi.org/10.1021/ci400065e | J. Chem. Inf. Model. 2013, 53, 982−996

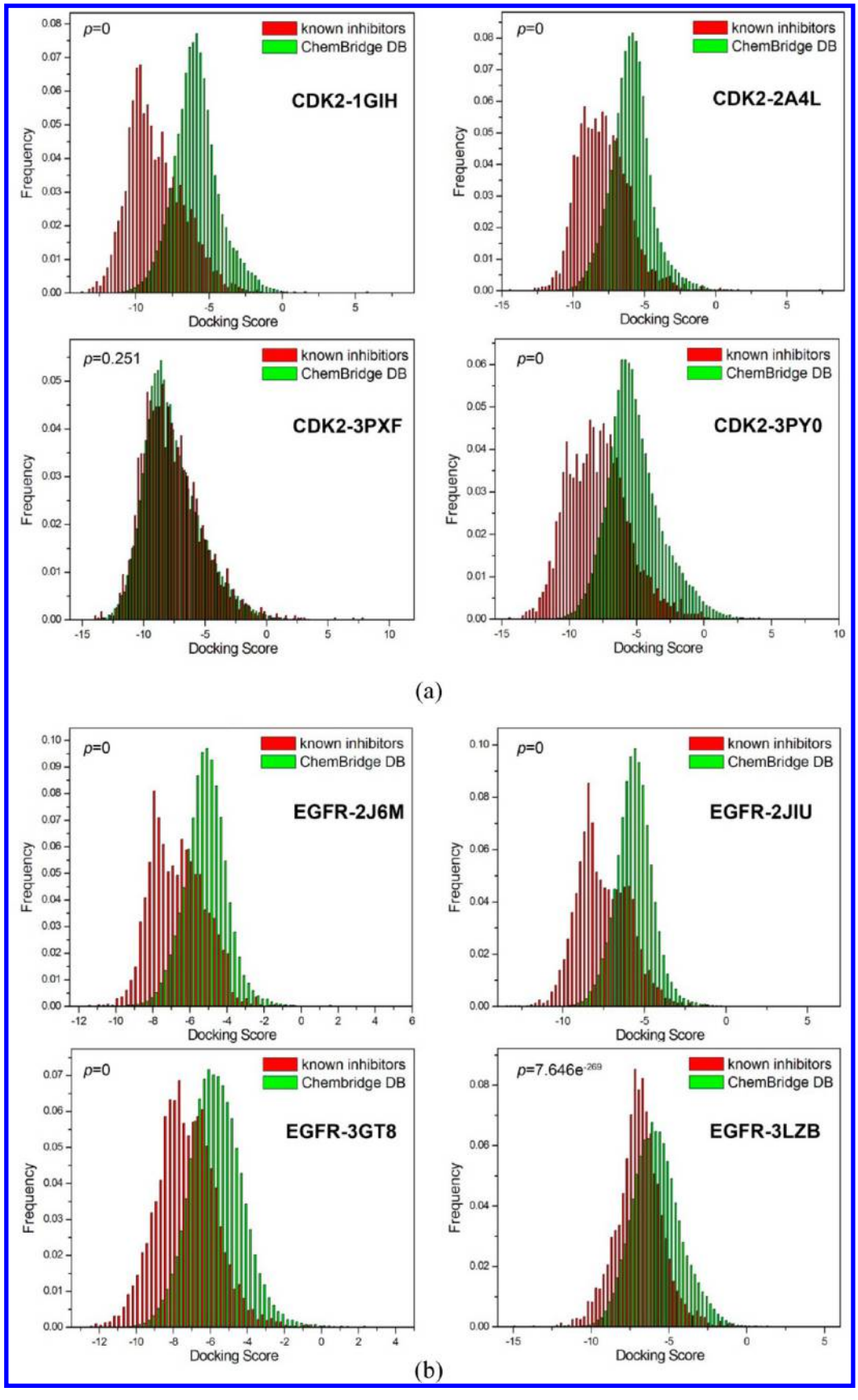


**Figure 4.** continued


dx.doi.org/10.1021/ci400065e | J. Chem. Inf. Model. 2013, 53, 982−996

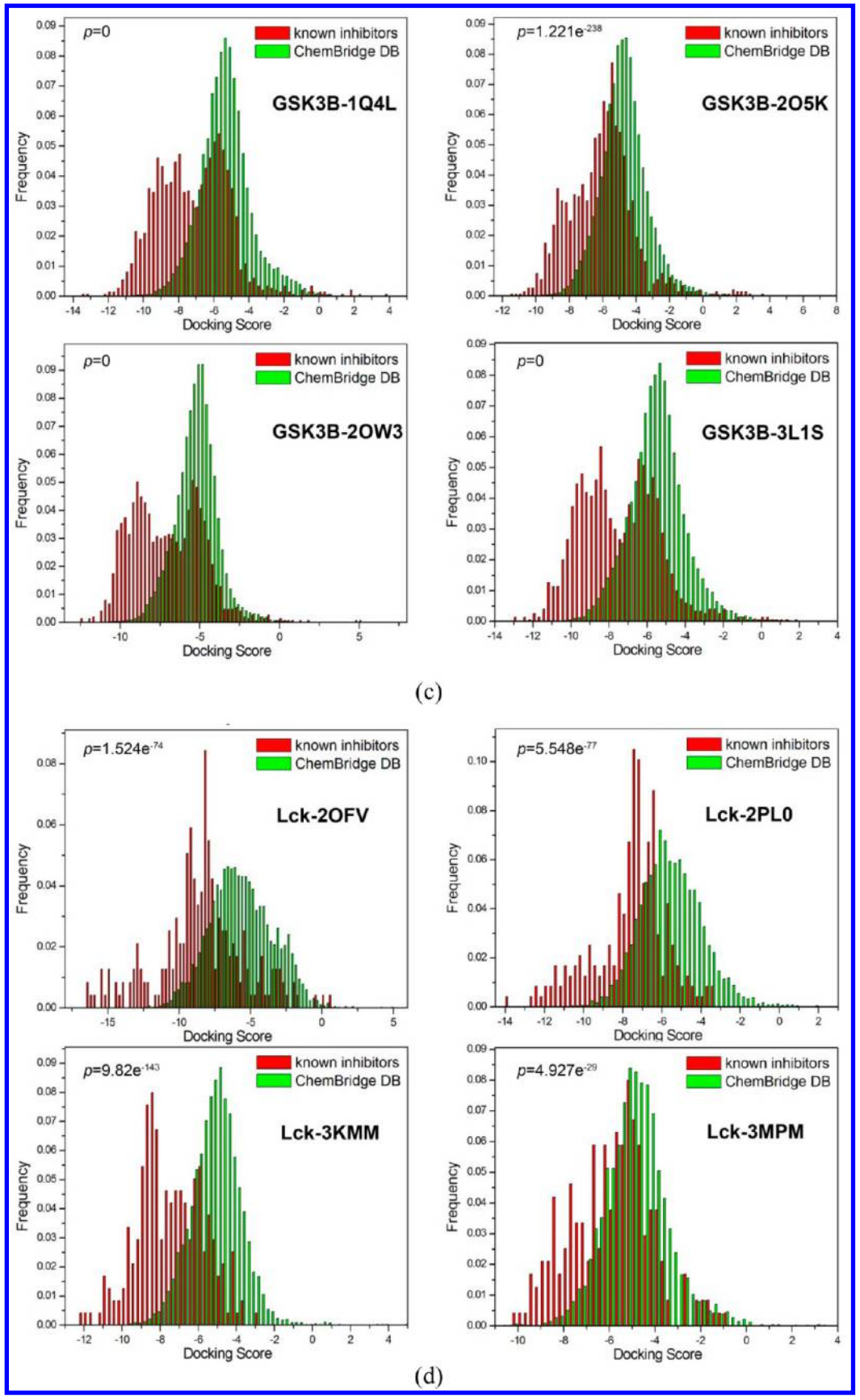


**Figure 4.** continued


dx.doi.org/10.1021/ci400065e | J. Chem. Inf. Model. 2013, 53, 982−996

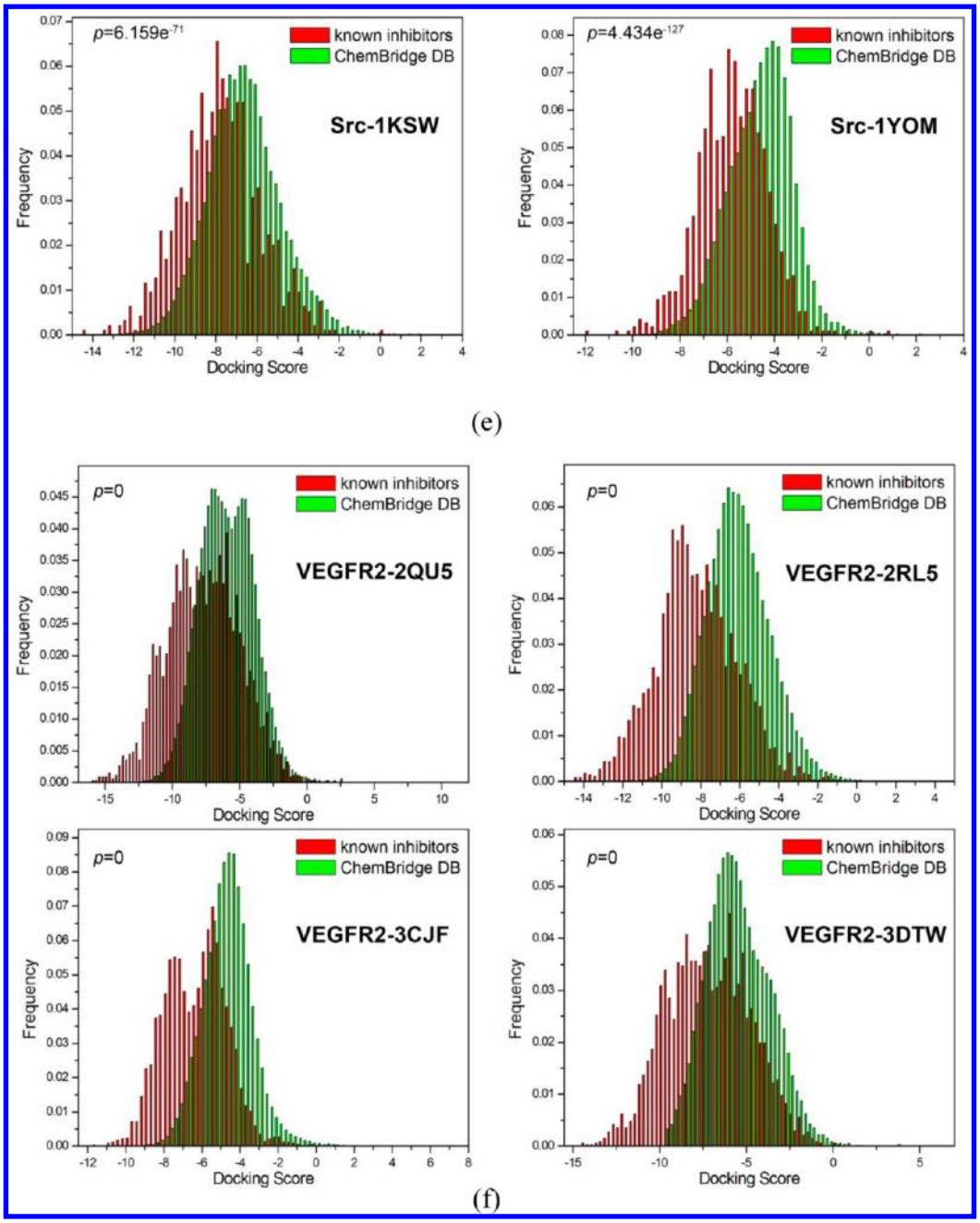


**Figure 4.** Distributions of the XP scores of the inhibitors and noninhibitors for (a) CDK2, (b) EGFR, (c) GSK3B, (d) Lck, (e) VEGFR, (e) Src, and (f) VEGFR2.

(Figure S3b), we can observe that 3LZB shows a longer and narrower binding site than 2JIU. This may be primarily explained by the strong H-bonding interactions between ITI and Lys721, Met769, and Thr830. The volumes of the binding pockets measured by SiteMap are 456.12 and 429.44 Å$^3$ for 2JIU and 3LZB, respectively. Although the volume of the 3LZB binding pocket is only slightly smaller than that of the 2JIU binding pocket, the narrower binding pocket of 3LZB still hinders the binding of some molecules.

**GSK3B Kinase.** As the schematic representation of the interactions shown in Supporting Information Figure S3c, the inhibitor (HBM) in 2O5K forms three H-bonds with the residues Asp133, Val135, and Arg220, and the inhibitor (Z92) in 3L1S forms four H-bonds with the residues Lys85, Asp133, Val135, and Arg220. The solvent-accessible surfaces of the ATP-binding pockets of 2O5K and 3L1S are illustrated in Figure S3c. The volumes of the ATP-binding pockets for 2O5K and 3L1S are 438.01 and 309.39 Å$^3$, respectively, suggesting that the difference of the conformational change of the binding pocket induced by different inhibitors is quite significant. In molecular docking calculations, the protein structure is rigid, and the larger binding pocket of 2O5K will be unfavorable for various inhibitors to form tight interactions with the target. Moreover, it is easier for those noninhibitors with low molecular weight to be docked into the larger binding pocket.

**Lck Kinase.** According to the schematic representation of the interactions shown in Supporting Information Figure S3d, there are three H-bonds between the inhibitor (5LK) in 3MPM and the residues Glu288, Thr316, and Met319 and two H-bonds between the inhibitor (LHL) in 3KMM and the residue


dx.doi.org/10.1021/ci400065e | J. Chem. Inf. Model. 2013, 53, 982−996

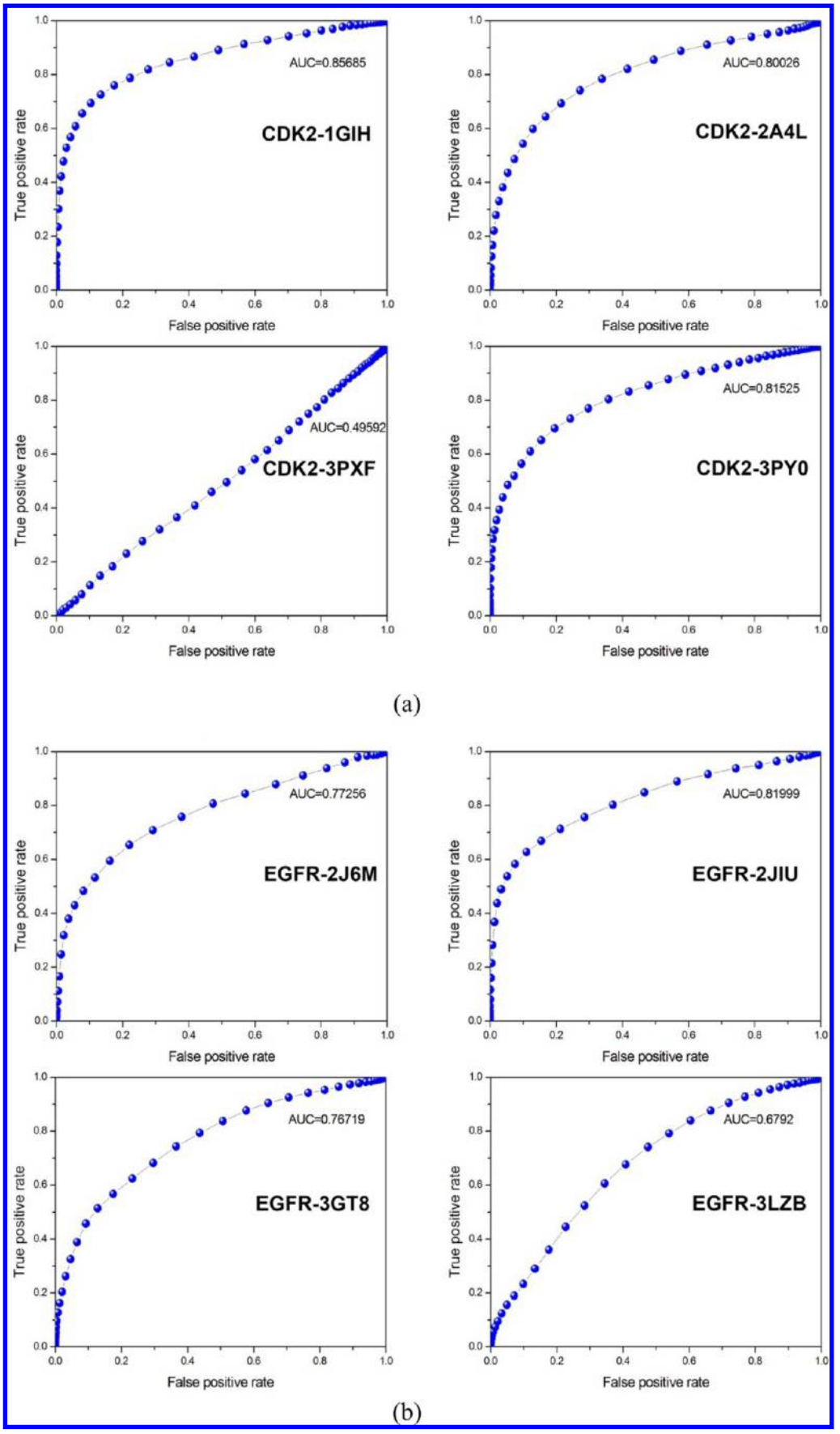


**Figure 5.** continued


dx.doi.org/10.1021/ci400065e | *J. Chem. Inf. Model.* 2013, 53, 982−996

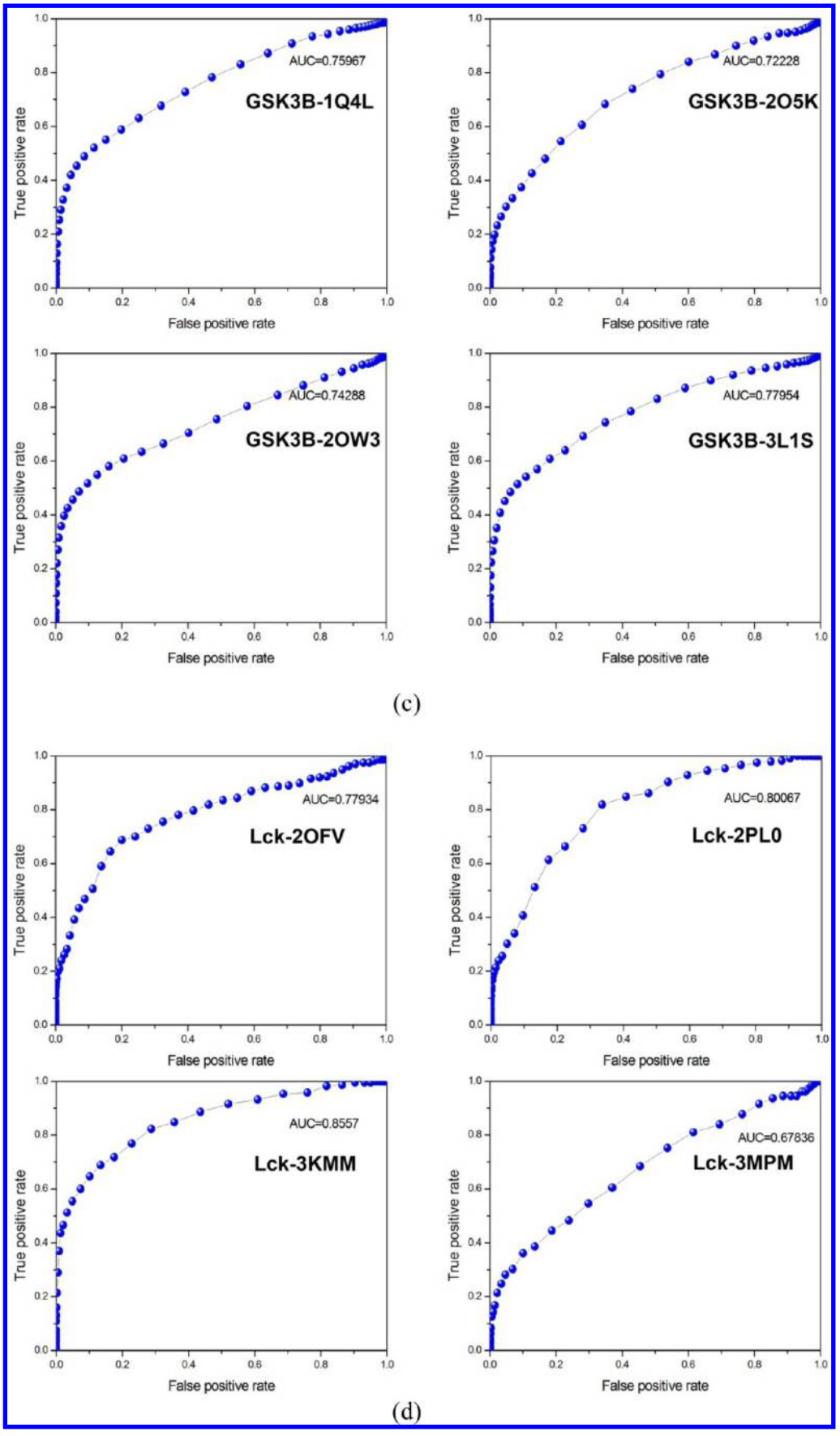


**Figure 5.** continued


dx.doi.org/10.1021/ci400065e | *J. Chem. Inf. Model.* 2013, 53, 982−996

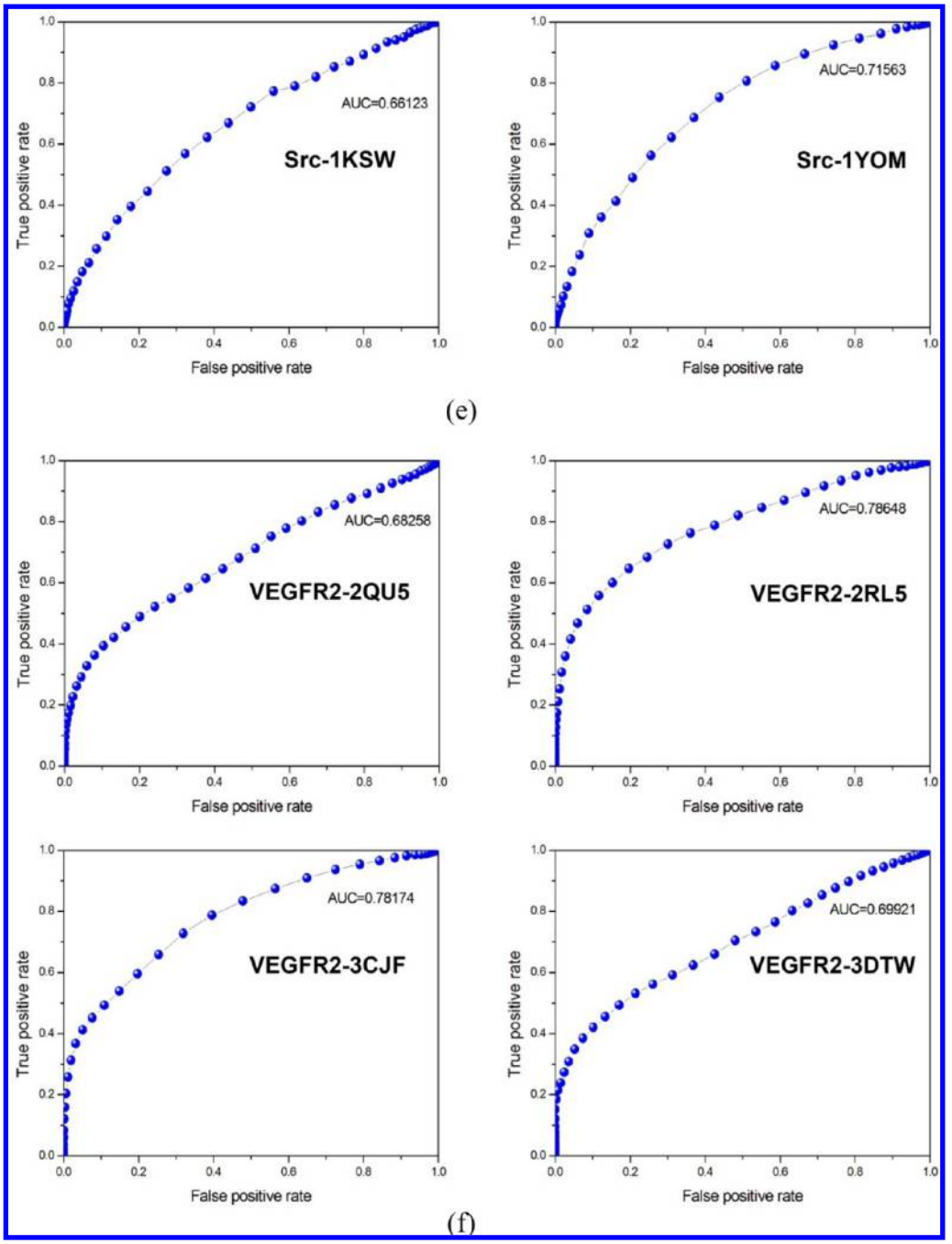


**Figure 5.** ROC curves for the performance of molecular docking to distinguish the inhibitors from noninhibitors for (a) CDK2, (b) EGFR, (c) GSK3B, (d) Lck, (e) VEGFR, (e) Src, and (f) VEGFR2.

Met319. Moreover, LHL forms the $\sigma-\pi$ interaction with Lys273 in 3KMM. The volumes of 3KMM and 3MPM are 255.54 and 397.88 Å$^3$, respectively. Therefore, similar to GSK3B, the larger ATP-binding pocket of 3MPM is unfavorable for some inhibitors to form tight binding.

**Src Kinase.** The schematic representations of the interactions (Supporting Information Figure S3c) show that there are three H-bonds between the inhibitor (NBS) in 1KSW and the residues Lys295, Glu339, and Met341 and two H-bonds between the inhibitor (P01) in 1YOM and the residue Met343. The volumes of the pockets for 1KSW and 1YOM are 519.30 and 300.47 Å$^3$, respectively. Obviously, the responds of the ATP-binding pockets to the binding of different inhibitors are quite different. Unfortunately, the molecular docking calculations based on 1YOM or 1KSW cannot give valid predictions.

**VEGFR2 Kinase.** The schematic representation of the interactions shows that the inhibitor (276) in 2QU5 forms more H-bonds than the inhibitor (2RL) in 2RL5. Moreover, the inhibitor (276) in 2QU5 exhibits strong $\sigma-\pi$ interactions with Lys868 in 2QU5. It is obvious that the inhibitor 276 forms tighter interactions with the VEGFR2 kinase than the inhibitor 2RL. According to the calculations of SiteMap, the volumes of the binding pockets for 2QU5 and 2RL5 are 385.53 and 630.78 Å$^3$, respectively. Similar to CDK2, it appears that the compact ATP-binding pocket of 2QU5 will hinder the entrance of some inhibitors into the binding pocket.


dx.doi.org/10.1021/ci400065e | J. Chem. Inf. Model. 2013, 53, 982−996

Our results demonstrate that the performance of molecular docking is quite sensitive to the protein structures used for the calculations and the proper volume and shape of the binding site are essential for achieving accurate predictions. Therefore, if multiple structures with large conformational diversity are available for the same target, we should compare the performance of the predictions for different protein structures and choose the best one. Certainly, we can use multiple structures of the same target in docking calculations, and it is possible that the predictions from different structures complement each other and the induce-fit effect can be minimized.

**Molecular Docking for Predicting Dual-Target Inhibitors.** After validating the performance of molecular docking for individual targets, the performance of molecular docking to predict dual-target inhibitors was evaluated. First, the single crystal protein structure for each target with the best docking performance was used for predicting dual-target inhibitors. The compound set that consists of the inhibitors of two targets and noninhibitors was docked into the proteins and scored using the Glide XP mode. The prediction results of the dual inhibitors are summarized in Table 2. Different cutoffs were used to distinguish the inhibitors from noninhibitors for each protein. First, the cutoff values identified by RP in the previous sections were used. Obviously, the RP cutoffs produce too many hits. For example, for the CDK2-GSK3B pair, the number of the dual-target inhibitors is 2208. Although 41.1% of known dual-target inhibitors were successfully predicted, but the prediction accuracy is quite low (5.25%) due to the high false positives rate. Then, three different cutoffs, including the top 10%, 5%, and 3%, were used. As shown in Table 2, false positives were significantly reduced by adjusting the cutoff values of docking scores for individual proteins. If a more stringent cutoff was used, the number of false positives is reduced significantly; however, the yields are reduced correspondingly. For example, for the CDK2-GSK3B pair, when employing the cutoffs of the top 5% and 3%, the number of the false positives decreases from 471 to 238, but the yield also decreases from 18.1% to 6.03%.

The discussions in the previous section show that the accuracy of docking is sensitive to different crystal structures. Using multiple structures of the same protein with enough conformational diversity may enhance the accuracy of molecular docking.[47] Then, docking to the multiple structures for each protein was employed to search dual-target inhibitors. The results from independent runs for different structures were merged and used to predict the dual-target inhibitors (Table 2). Compared with the docking results based on single structures, those based on multiple structures of the same protein give higher yields; that is to say, more true dual inhibitors were successfully included in the final list. For example, based on the top 5% cutoff, for the CDK2-GSK3B pair, 36.9% of true dual-target inhibitors were successfully predicted by the docking to multiple structures, while only 18.1% by the docking to the single structures. In the mean time, the utility of multiple structures increases false positives, and may even decreases prediction accuracies. As shown in Table 2, the CDK2-GSK3B and Lck-VEGFR2 kinase pairs show higher yields of dual inhibitors than the others. The low yields of the dual inhibitors for the EGFR-Src and Lck-Src pairs are obviously related to the bad performance of molecular docking for the Src and Lck kinases. According to the data shown in Table 1, the XP scores given by Glide cannot effectively distinguish the inhibitors from the noninhibitors for Src and Lck.

As shown in Table 2, the prediction accuracies for the four pairs are relatively low, which is obviously caused by the high false hit rates. For example, for the CDK2-GSK3B pair, the number of the dual inhibitors predicted by molecular docking based on the top 5% cutoff are 1379, among which 1275 are false positives. In these 1275 false positives, 747 are the inhibitors of CDK2 while the noninhibitors of GSK3B, 309 are the inhibitors of GSK3B while the noninhibitors of CDK2, and 219 are the noninhibitors of both GSK3B and CDK2. That is to say, many inhibitors only targeted to a single protein were predicted to be dual inhibitors. The bad prediction for target selectivity may be partially explained by the fact that the ATP-binding sites of the kinases in each kinase pair are quite conserved in sequences and structures. Moreover, the quality of the data is another issue for high false positive rates. It is possible that some true inhibitors of kinases were not collected by BindingDB or have not been tested by experiment.

## CONCLUSION

In the present study, we evaluated the performance of molecular docking to distinguish dual-target inhibitors from nondual-target inhibitors for four kinase pairs. First, structural clustering was used to find the most representative structures for each kinase target. The performance of molecular docking to predict the inhibitors for individual kinases was evaluated, and we found that the prediction accuracy is sensitive to protein structures used for molecular docking. Then, the performance of molecular docking to predict dual-target inhibitors was assessed. Our results show that most noninhibitors can be successfully filtered and the dual inhibitors of two kinase pairs can be predicted well, but the prediction accuracy is still limited due to high rate of false positives. Therefore, it seems that for some systems molecular docking still cannot give reliable predictions to find inhibitors of two targets with similar binding pockets. At the current stage, how to improve the prediction for target selectivity is still a big challenge. One possible way to improve the prediction accuracy for target selectivity is to develop consensus models by combining our method with other approaches.

## ASSOCIATED CONTENT

### Supporting Information

Table S1: volumes of the multiple crystal structures for each target. Figure S1: flowchart of the protocol for ligand preparations. Figure S2: comparisons of the binding pose of the ligand in the crystal complex (green) and the docked pose (magenta) predicted by Glide with the XP scoring mode for (a) 3CJF, (b) 3GT8, and (c) 3LZB. Figure S3: schematic representations of the interactions and Connolly surfaces of the crystal structures with the best and worst performance for (a) CDK2, (b) EGFR, (c) GSK3B, (d) Lck, (e) VEGFR, (e) Src, and (f) VEGFR2. Figure S4: (a) distributions of the XP docking scores of the inhibitors and noninhibitors of 1GIH predicted by the docking based on the ATP-binding site; (b) ROC curve for the performance of molecular docking to distinguish the inhibitors from noninhibitors for 1GIH. This material is available free of charge via the Internet at http://pubs.acs.org.

## AUTHOR INFORMATION

### Corresponding Author

*E-mail: tingjunhou@hotmail.com. Phone: +86-512-65882039.

### Notes

The authors declare no competing financial interest.

## ■ ACKNOWLEDGMENTS

This study was supported by the National Science Foundation of China (21173156), the National Basic Research Program of China (973 program, 2012CB932600), and the Priority Academic Program Development of Jiangsu Higher Education Institutions (PAPD).

## ■ REFERENCES

(1) Drews, J. Drug discovery: A historical perspective. *Science* **2000**, *287*, 1960−1964.
(2) Morphy, R. Selectively Nonselective Kinase Inhibition: Striking the Right Balance. *J. Med. Chem.* **2010**, *53*, 1413−1437.
(3) Keith, C. T.; Borisy, A. A.; Stockwell, B. R. Multicomponent therapeutics for networked systems. *Nat. Rev. Drug Discov.* **2005**, *4*, 71−78.
(4) Zimmermann, G. R.; Lehar, J.; Keith, C. T. Multi-target therapeutics: when the whole is greater than the sum of the parts. *Drug Discov. Today* **2007**, *12*, 34−42.
(5) Csermely, P.; Agoston, V.; Pongor, S. The efficiency of multi-target drugs: the network approach might help drug design. *Trends Pharmacol. Sci.* **2005**, *26*, 178−182.
(6) Morphy, R.; Kay, C.; Rankovic, Z. From magic bullets to designed multiple ligands. *Drug Discov. Today* **2004**, *9*, 641−651.
(7) Thangapandian, S.; John, S.; Sakkiah, S.; Lee, K. W. Molecular Docking and Pharmacophore Filtering in the Discovery of Dual-Inhibitors for Human Leukotriene A4 Hydrolase and Leukotriene C4 Synthase. *J. Chem. Inf. Model.* **2011**, *51*, 33−44.
(8) Capdeville, R.; Buchdunger, E.; Zimmermann, J.; Matter, A. Glivec (ST1571, Imatinib), a rationally developed, targeted anticancer drug. *Nat. Rev. Drug Discov.* **2002**, *1*, 493−502.
(9) Motzer, R. J.; Michaelson, M. D.; Redman, B. G.; Hudes, G. R.; Wilding, G.; Figlin, R. A.; Ginsberg, M. S.; Kim, S. T.; Baum, C. M.; DePrimo, S. E.; Li, J. Z.; Bello, C. L.; Theuer, C. P.; George, D. J.; Rini, B. I. Activity of SU11248, a multitargeted inhibitor of vascular endothelial growth factor receptor and platelet-derived growth factor receptor, in patients with metastatic renal cell carcinoma. *J. Clin. Oncol.* **2006**, *24*, 16−24.
(10) Wilhelm, S.; Carter, C.; Lynch, M.; Lowinger, T.; Dumas, J.; Smith, R. A.; Schwartz, B.; Simantov, R.; Kelley, S. Discovery and development of sorafenib: a multikinase inhibitor for treating cancer. *Nat. Rev. Drug Discov.* **2006**, *5*, 835−844.
(11) Quintas-Cardama, A.; Kantarjian, H.; Jones, D.; Nicaise, C.; O'Brien, S.; Giles, F.; Talpaz, M.; Cortes, J. Dasatinib (BMS-354825) is active in Philadelphia chromosome-positive chronic myelogenous leukemia after imatinib and nilotinib (AMN 107) therapy failure. *Blood* **2007**, *109*, 497−499.
(12) Wood, E. R.; Truesdale, A. T.; McDonald, O. B.; Yuan, D.; Hassell, A.; Dickerson, S. H.; Ellis, B.; Pennisi, C.; Horne, E.; Lackey, K.; Alligood, K. J.; Rusnak, D. W.; Gilmer, T. M.; Shewchuk, L. A unique structure for epidermal growth factor receptor bound to GW572016 (Lapatinib): Relationships among protein conformation, inhibitor off-rate, and receptor activity in tumor cells. *Cancer Res.* **2004**, *64*, 6652−6659.
(13) Scapin, G. Structural biology in drug design: selective protein kinase inhibitors. *Drug Discov. Today* **2002**, *7*, 601−611.
(14) Kinnings, S. L.; Jackson, R. M. Binding Site Similarity Analysis for the Functional Classification of the Protein Kinase Family. *J. Chem. Inf. Model.* **2009**, *49*, 318−329.
(15) Fabian, M. A.; Biggs, W. H.; Treiber, D. K.; Atteridge, C. E.; Azimioara, M. D.; Benedetti, M. G.; Carter, T. A.; Ciceri, P.; Edeen, P. T.; Floyd, M.; Ford, J. M.; Galvin, M.; Gerlach, J. L.; Grotzfeld, R. M.; Herrgard, S.; Insko, D. E.; Insko, M. A.; Lai, A. G.; Lelias, J. M.; Mehta, S. A.; Milanov, Z. V.; Velasco, A. M.; Wodicka, L. M.; Patel, H. K.; Zarrinkar, P. P.; Lockhart, D. J. A small molecule-kinase interaction map for clinical kinase inhibitors. *Nat. Biotechnol.* **2005**, *23*, 329−336.
(16) Fedorov, O.; Marsden, B.; Pogacic, V.; Rellos, P.; Mueller, S.; Bullock, A. N.; Schwaller, J.; Sundstrom, M.; Knapp, S. A systematic interaction map of validated kinase inhibitors with Ser/Thr kinases. *Proc. Natl. Acad. Sci. U.S.A.* **2007**, *104*, 20523−20528.
(17) Karaman, M. W.; Herrgard, S.; Treiber, D. K.; Gallant, P.; Atteridge, C. E.; Campbell, B. T.; Chan, K. W.; Ciceri, P.; Davis, M. I.; Edeen, P. T.; Faraoni, R.; Floyd, M.; Hunt, J. P.; Lockhart, D. J.; Milanov, Z. V.; Morrison, M. J.; Pallares, G.; Patel, H. K.; Pritchard, S.; Wodicka, L. M.; Zarrinkar, P. P. A quantitative analysis of kinase inhibitor selectivity. *Nat. Biotechnol.* **2008**, *26*, 127−132.
(18) Posy, S. L.; Hermsmeier, M. A.; Vaccaro, W.; Ott, K.-H.; Todderud, G.; Lippy, J. S.; Trainor, G. L.; Loughney, D. A.; Johnson, S. R. Trends in Kinase Selectivity Insights for Target Class-Focused Library Screening. *J. Med. Chem.* **2011**, *54*, 54−66.
(19) Smyth, L. A.; Collins, I. Measuring and interpreting the selectivity of protein kinase inhibitors. *J. Chem. Biol.* **2009**, *2*, 131−51.
(20) Goldstein, D. M.; Gray, N. S.; Zarrinkar, P. P. High-throughput kinase profiling as a platform for drug discovery. *Nat. Rev. Drug Discov.* **2008**, *7*, 391−397.
(21) Sheridan, R. P.; Nam, K.; Maiorov, V. N.; McMasters, D. R.; Cornell, W. D. QSAR Models for Predicting the Similarity in Binding Profiles for Pairs of Protein Kinases and the Variation of Models between Experimental Data Sets. *J. Chem. Inf. Model.* **2009**, *49*, 1974−1985.
(22) Niijima, S.; Shiraishi, A.; Okuno, Y. Dissecting Kinase Profiling Data to Predict Activity and Understand Cross-Reactivity of Kinase Inhibitors. *J. Chem. Inf. Model.* **2012**, *52*, 901−912.
(23) Sciabola, S.; Stanton, R. V.; Wittkopp, S.; Wildman, S.; Moshinsky, D.; Potluri, S.; Xi, H. Predicting kinase selectivity profiles using free-Wilson QSAR analysis. *J. Chem. Inf. Model.* **2008**, *48*, 1851−1867.
(24) Martin, E.; Mukherjee, P.; Sullivan, D.; Jansen, J. Profile-QSAR: A Novel meta-QSAR Method that Combines Activities across the Kinase Family To Accurately Predict Affinity, Selectivity, and Cellular Activity. *J. Chem. Inf. Model.* **2011**, *51*, 1942−1956.
(25) Zhang, X.; Fernandez, A. In silico drug profiling of the human kinome based on a molecular marker for cross reactivity. *Mol. Pharmaceutics* **2008**, *5*, 728−738.
(26) Lapins, M.; Wikberg, J. E. S. Kinome-wide interaction modelling using alignment-based and alignment-independent approaches for kinase description and linear and non-linear data analysis techniques. *BMC Bioinf.* **2010**, *11*, 339−354.
(27) Martin, E.; Mukherjee, P. Kinase-Kernel Models: Accurate In silico Screening of 4 Million Compounds Across the Entire Human Kinome. *J. Chem. Inf. Model.* **2012**, *52*, 156−170.
(28) Ma, X. H.; Wang, R.; Tan, C. Y.; Jiang, Y. Y.; Lu, T.; Rao, H. B.; Li, X. Y.; Go, M. L.; Low, B. C.; Chen, Y. Z. Virtual Screening of Selective Multitarget Kinase Inhibitors by Combinatorial Support Vector Machines. *Mol. Pharmaceutics* **2010**, *7*, 1545−1560.
(29) Gozalbes, R.; Simon, L.; Froloff, N.; Sartori, E.; Monteils, C.; Baudelle, R. Development and experimental validation of a docking strategy for the generation of kinase-targeted libraries. *J. Med. Chem.* **2008**, *51*, 3124−3132.
(30) Ma, X. H.; Shi, Z.; Tan, C.; Jiang, Y.; Go, M. L.; Low, B. C.; Chen, Y. Z. In-Silico Approaches to Multi-target Drug Discovery. *Pharm. Res.* **2010**, *27*, 739−749.
(31) Liu, T.; Lin, Y.; Wen, X.; Jorissen, R. N.; Gilson, M. K. BindingDB: a web-accessible database of experimentally determined protein-ligand binding affinities. *Nucleic Acids Res.* **2007**, *35*, D198−D201.
(32) Desai, P. V.; Patny, A.; Sabnis, Y.; Tekwani, B.; Gut, J.; Rosenthal, P.; Srivastava, A.; Avery, M. Identification of novel parasitic cysteine protease inhibitors using virtual screening. 1. The ChemBridge database. *J. Med. Chem.* **2004**, *47*, 6609−6615.
(33) Berman, H. M.; Westbrook, J.; Feng, Z.; Gilliland, G.; Bhat, T. N.; Weissig, H.; Shindyalov, I. N.; Bourne, P. E. The Protein Data Bank. *Nucleic Acids Res.* **2000**, *28*, 235−242.
(34) Cozzini, P.; Kellogg, G. E.; Spyrakis, F.; Abraham, D. J.; Costantino, G.; Emerson, A.; Fanelli, F.; Gohlke, H.; Kuhn, L. A.;

Morris, G. M.; Orozco, M.; Pertinhez, T. A.; Rizzi, M.; Sotriffer, C. A. Target Flexibility: An Emerging Consideration in Drug Discovery and Design. *J. Med. Chem.* **2008**, *51*, 6237−6255.
(35) Russell, R. B.; Barton, G. J. Multiple protein sequence alignment from tertiary structure comparison: Assignment of global and residue confidence levels. *Proteins−Struct. Funct. Genet.* **1992**, *14*, 309−323.
(36) Humphrey, W.; Dalke, A.; Schulten, K. VMD: Visual molecular dynamics. *J. Molec. Graph. Modell.* **1996**, *14*, 33−38.
(37) Leng, L.; Chen, L.; Fan, J.; Greven, D.; Arjona, A.; Du, X.; Austin, D.; Kashgarian, M.; Yin, Z.; Huang, X. R. A small-molecule macrophage migration inhibitory factor antagonist protects against glomerulonephritis in lupus-prone NZB/NZW F1 and MRL/lpr mice. *J. Immunol.* **2011**, *186*, 527−538.
(38) Kaminski, G. A.; Friesner, R. A.; Tirado-Rives, J.; Jorgensen, W. L. Evaluation and reparametrization of the OPLS-AA force field for proteins via comparison with accurate quantum chemical calculations on peptides. *J. Phys. Chem. B* **2001**, *105*, 6474−6487.
(39) Brown, F. G.; Nikolic-Paterson, D. J.; Hill, P. A.; Isbel, N. M.; Dowling, J.; Metz, C. M.; Atkins, R. C. Urine macrophage migration inhibitory factor reflects the severity of renal injury in human glomerulonephritis. *J. Am. Soc. Nephrol.* **2002**, *13*, S7−S13.
(40) *Discovery Studio 2.5 Guide*; Accelrys Inc., San Diego, 2009, http://www.accelrys.com.
(41) Yan, X.; Xue-jun, L. Multi-target therapeutics and new drug discovery. *Acta Pharmaceutica Sin.* **2009**, *44*, 226−230.
(42) *Schrödinger*, version 9.0; Schrödinger, LLC, New York, NY, 2009, http://www.schrodinger.com.
(43) Friesner, R. A.; Banks, J. L.; Murphy, R. B.; Halgren, T. A.; Klicic, J. J.; Mainz, D. T.; Repasky, M. P.; Knoll, E. H.; Shelley, M.; Perry, J. K.; Shaw, D. E.; Francis, P.; Shenkin, P. S. Glide: A new approach for rapid, accurate docking and scoring. 1. Method and assessment of docking accuracy. *J. Med. Chem.* **2004**, *47*, 1739−1749.
(44) Totrov, M.; Abagyan, R. Flexible ligand docking to multiple receptor conformations: a practical alternative. *Curr. Opin. Struct. Biol.* **2008**, *18*, 178−184.
(45) B-Rao, C.; Subramanian, J.; Sharma, S. D. Managing protein flexibility in docking and its applications. *Drug Discov. Today* **2009**, *14*, 394−400.
(46) Sheridan, R.; McGaughey, G.; Cornell, W. Multiple protein structures and multiple ligands: effects on the apparent goodness of virtual screening results. *J. Comput.-Aided Molec. Des.* **2008**, *22*, 257−265.
(47) Santiago, D. N.; Pevzner, Y.; Durand, A. A.; Tran, M.; Scheerer, R. R.; Daniel, K.; Sung, S. S.; Lee Woodcock, H.; Guida, W. C.; Brooks, W. H. Virtual Target Screening: Validation Using Kinase Inhibitors. *J. Chem. Inf. Model.* **2012**, *52*, 2192−2203.
(48) Bottegoni, G.; Rocchia, W.; Rueda, M.; Abagyan, R.; Cavalli, A. Systematic Exploitation of Multiple Receptor Conformations for Virtual Ligand Screening. *PLoS ONE* **2012**, *6*, e18845.
(49) Betzi, S.; Alam, R.; Martin, M.; Lubbers, D. J.; Han, H.; Jakkaraj, S. R.; Georg, G. I.; Schoenbrunn, E. Discovery of a Potential Allosteric Ligand Binding Site in CDK2. *ACS Chem. Biol.* **2011**, *6*, 492−501.